catalysts

MDPI

Article

Gram-Scale Synthesis of CoO/C as Base for PtCo/C High-Performance Catalysts for the Oxygen Reduction Reaction

Dmitry Mauer [1], Sergey Belenov [1,2], Vladimir Guterman [1,*], Anatoly Nikolsky [3], Alexey Kozakov [3], Alexey Nikulin [1], Danil Alexeenko [1,2] and Olga Safronenko [1]

[1] Chemistry Faculty, Southern Federal University, 344090 Rostov-on-Don, Russia; mauer@sfedu.ru (D.M.); sbelenov@sfedu.ru (S.B.); aynikulin@sfedu.ru (A.N.); dvalekseenko@sfedu.ru (D.A.); osafronenko@sfedu.ru (O.S.)
[2] Prometheus R&D LLC, 4g/36 Zhmaylova St., 344091 Rostov-on-Don, Russia
[3] Institute of Physics, Southern Federal University, 344006 Rostov-on-Don, Russia; anikolskiy@sfedu.ru (A.N.); atkozakov@sfedu.ru (A.K.)
* Correspondence: guter@sfedu.ru

Abstract: The composition, structure, catalytic activity in the ORR and stability of PtCo/C materials, obtained in two stages and compared with commercial Pt/C analogs, were studied. At the first stage of the synthesis performed by electrodeposition of cobalt on a carbon support, a CoO_x/C composite containing 8% and 25 wt% cobalt oxide was successfully obtained. In the second step, $PtCoO_x$/C catalysts of Pt1.56Co and Pt1.12Co composition containing 14 and 30 wt% Pt, respectively, were synthesized based on the previously obtained composites. According to the results of the composition and structure analysis of the obtained $PtCoO_x$/C catalysts by X-ray diffraction (XRD), X-ray fluorescence analysis (XRF), transmission electron microscopy (TEM) and X-ray photoelectron spectroscopy (XPS) methods, the formation of small bimetallic nanoparticles on the carbon support surface has been proved. The resulting catalysts demonstrated up to two times higher specific catalytic activity in the ORR and high stability compared to commercial Pt/C analogs.

Keywords: PEMFC; electrocatalyst; PtCo/C; composite support; oxygen electroreduction; catalyst synthesis; catalyst durability; ESA

Citation: Mauer, D.; Belenov, S.; Guterman, V.; Nikolsky, A.; Kozakov, A.; Nikulin, A.; Alexeenko, D.; Safronenko, O. Gram-Scale Synthesis of CoO/C as Base for PtCo/C High-Performance Catalysts for the Oxygen Reduction Reaction. *Catalysts* **2021**, *11*, 1539. https://doi.org/10.3390/catal11121539

Academic Editor: Minhua Shao

Received: 17 November 2021
Accepted: 9 December 2021
Published: 17 December 2021

1. Introduction

In recent years, the technology of proton-exchange membrane fuel cells (PEMFC) has been intensively developed, as a result of its growing application in various vehicles [1]. Vehicles driven by the PEMFC have several important advantages over the classical vehicles based on internal combustion engines and battery-powered electric vehicles. No harmful emissions into the atmosphere, as well as a high degree of autonomy, range and quick refueling speed, are among the crucial benefits. The most significant problem with the fuel cells is their high cost [2], as a Pt-containing catalyst is one of the most expensive PEMFC components [3]. Reducing the platinum loading in the PEMFC, while maintaining or increasing its specific power and service life, is an important task for researchers nowadays [4,5].

One of the most promising approaches to improving the performance of catalysts is to replace pure platinum nanoparticles with the bimetallic nanoparticles obtained by alloying Pt with transition d-metals such as Co, Ni, Fe, Cu, etc. [6–9]. The increase in the electrocatalysts activity based on the doped platinum can be explained by the geometric factors (reduction of interatomic distance in the crystal lattice) [10], the change in the energy of platinum d-orbitals [11], as well as in the morphology of the NPs surface [12] due to the selective dissolution of the alloying component [8,13,14]. In [15] such an increase is associated with the catalytic activity of Pt_3Ni and Pt_3Co alloys in the oxygen reduction reaction (ORR) compared to pure Pt with the inhibition of the of Pt-OH_{ads} groups formation

at Pt sites surrounded by the "oxidized" Ni and Co atoms at potentials above 0.8 V. The Toyota company is known to use PtCo catalysts in the PEMFC production for the Mirai cars [16], thus proving the promising commercial perspectives of such systems.

A great number of the latest publications and research in the field of PtCo/C catalyst is devoted to improving chemical methods for the synthesis of Pt-Co nanoparticles on carbon support. The common methods of chemical synthesis are the solvothermal [17–20], polyol [21–23], borohydride [24–26], microemulsion [27,28], carbothermic ones, to name a few. [29,30]. The borohydride synthesis method is perhaps one of the simplest [24–26]. In [31] it was found that PtCo/C catalysts obtained by the borohydride and polyol synthesis methods had a larger electrochemically active surface area (ESA) and a smaller nanoparticle size, compared to similar materials which were obtained with hydrazine. In [25], it was shown that PtCo/C catalysts obtained by the borohydride method were characterized by a smaller particle size and a higher ESA value, as compared to materials obtained by the carbothermal method. However, the use of the borohydride method did not allow realizing a high alloying degree for PtCo nanoparticles, which negatively affected the activity in the ORR. Despite its simplicity, a number of serious drawbacks are inherent to the borohydride synthesis method. These include uneven distribution of particles over the surface of the support, poorly reproducible degree of doping, a high degree of particle agglomeration, and, consequently, relatively low ESA values of the catalyst [24]. Among the problems typical for the chemical methods for the synthesis of bimetallic catalysts is the scaling complexity, which is a serious one, characteristic of the transition period from the laboratory to industrial production.

To solve this problem, in recent years much attention has been paid to the development of gram-scale synthesis technologies [32–35]. Such methods make it possible to produce the amount of catalysts from one to several tens of grams in a single synthesis, or to carry out a flow synthesis with continuous production of the catalyst. However, there are some drawbacks to these methods as well. Thus, in the production technology for PdCoPt trimetallic materials proposed in [32], expensive precursors are used, e.g., acetylacetonates of cobalt, platinum, and palladium. In [33], platinum and nickel acetylacetonates are also used as precursors in the preparation of PtNi catalysts, and dimethyl diallyl ammonium chloride (DDAC) is used as a surfactant. In some cases, it is necessary to use complex technical devices, such as a flow reactor [34].

Electrodeposition is one of the promising methods for producing metals and alloys, allowing the realization of a controlled gram-scale synthesis. A number of papers has been published about platinum electrodeposition on various carbon carriers: glass carbon [36,37], carbon nanotubes [38,39], technical carbon [40,41], carbon cloth or paper [42–44]. In [43], electrochemical deposition of Pt nanoparticles with a narrow dimensional distribution from Pt solution [$Pt(OH)_6$] was shown, based on the mode of pulse potential change. To the best of our knowledge, nobody has succeeded yet in obtaining Pt/C materials with the large ESA and high catalytic activity by electrodeposition of platinum onto carbon particles in suspension [45]. Another electrochemical approach to the synthesis of composite metal oxide/carbon carriers is a pulsed electrochemical dispersion of a metal electrode in a carbon suspension [46]. Depending on the nature of the metal, the metal (Pt) or oxide (Ni, Ti, Sn) particles formed during the dispersion process, deposit on the carbon support. At the same time, when using electrochemical dispersion, large platinum nanoparticles are formed, resulting in low Pt/C ESA materials. Thus, production of platinum NPs alloys with the help of d-metals, still remains very problematic.

In [47,48] we have developed methods for electrolytic production of composite SnO_2/C and SnNi/C materials. In the materials, which were obtained with the described method, the particles of the metal oxide were very small in size and were evenly distributed over the surface of the carbon support [49]. Platinum catalysts based on the composite SnO_2/C support showed high characteristics, primarily, in the reactions of electrooxidation of organic substances [50]. We believe, that CoO_x/C gram-scale composite materials obtained by electrolytic application of cobalt to the surface of micro/nanocarbon

particles could also be of interest when they are used as supports in the preparation of platinum-containing catalysts.

The objectives of this work are to obtain nanostructured CoO_x/C-materials and platinum-containing catalysts, produced on their basis; to study the composition, microstructure, stability and activity in the ORR of the obtained platinum-containing electrocatalysts.

2. Results and Discussion

Characteristics of Bimetallic Catalysts

CoOx/C materials with a mass fraction of oxide 8% (CC1 material) and 25% (CC2 material) were obtained by electrodeposition, as described in the Experimental section. Upon receipt of the CC1 sample, electrodeposition was carried out for 7 min at a current of 1A, upon receipt of the CC2 sample—12 min at a current of 0.8 A. On the diffraction patterns of the obtained samples (Figure 1a), there was a reflection of the carbon carrier and only one low intensity peak which could be attributed to the CoO phase. However, when studying the annealed residue of CoO_x/C samples, there were clearly visible sharp peaks of the Co_3O_4 phase in the diffractograms (Figure 1b). The XRD results for the annealed CoO/C samples allowed us to draw conclusions about the presence of a cobalt-containing X-ray amorphous oxide phase in the materials obtained by the electrodeposition method. Note that the technique used allows one to obtain gram quantities of a cobalt-containing support and use suspensions of different carbon materials.

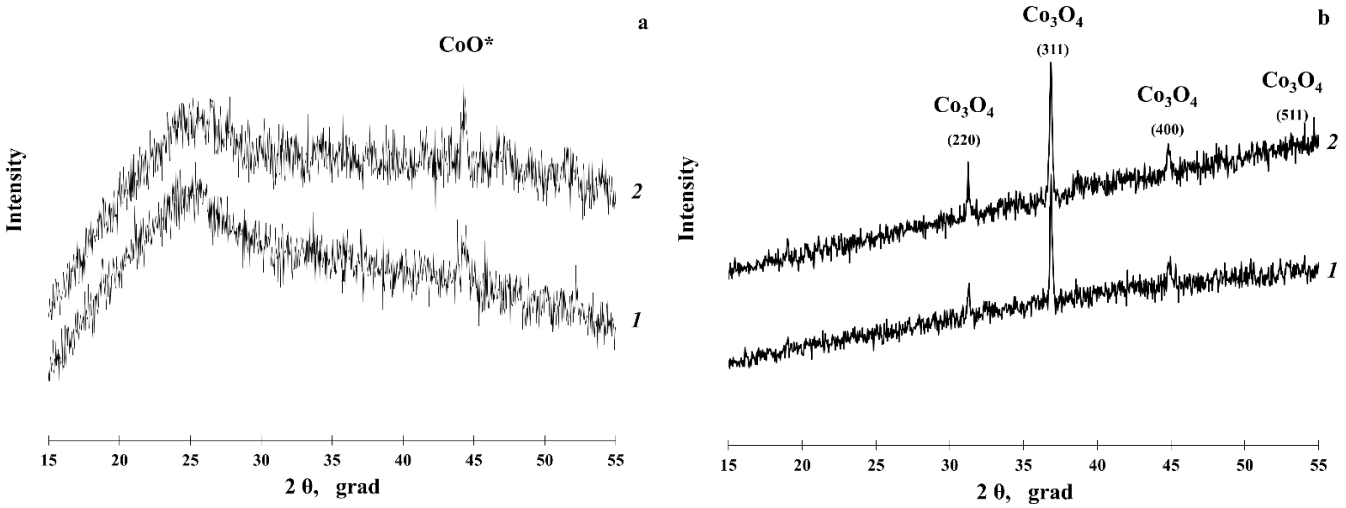

Figure 1. XRD patterns of materials: (**a**) 1—CoO/C—8% and 2—CoO/C—25%, (**b**) XRD patterns of materials 1—CoO/C—8% and 2—CoO/C—25% after high temperature oxidation. * An approximate interpretation due to the presence of only one reflection of the CoO phase in the X-ray diffractogram.

Platinum nanoparticles were supported on CC1 and CC2 carriers by the liquid-phase borohydride synthesis (see the Experimental section). The amount of H_2PtCl_6 in the initial solution was calculated so that, upon complete reduction of the platinum precursor, the atomic ratio of Pt: Co in the resulting material was 1:1. The calculated content of platinum in the catalysts was 17% and 32%, respectively, but the real mass fraction of Pt in PCC1 and PCC2 turned out to be slightly less and amounted to 14% and 30%, respectively (Table 1). The atomic ratio of Pt–Co in the samples, determined from XRF data, also differed from the calculated one (Table 1). Apparently, this indicates the loss of a part of cobalt during the synthesis of PCC1 and PCC2.

Table 1. Some composition and structure parameters of PtCo/C and commercial Pt/C materials.

Sample	ω(Pt), %.	Metal Composition (According to XRF)	Metal Composition (According to XRD)	Lattice Parameter of the Metal Component a, Å	Average crystallite size (XRD) Pt, nm
PCC1	14 ± 0.28	$Pt_{1.56}Co$	$Pt_{0.86}Co$	3.875	2.6 ± 0.2
PCC2	30 ± 0.6	$Pt_{1.12}Co$	$Pt_{0.86}Co$	3.876	3.3 ± 0.3
JM20	20 ± 0.4	-	-	3.923	2.3 ± 0.2
JM40	40 ± 0.8	-	-	3.923	3.0 ± 0.3

XRD patterns of PtCo/C materials (Figure 2) make it possible to identify the carbon phase by reflection C (002) at a 2θ of about 25 degrees, and the platinum phase by reflections Pt (111) and Pt (200) at 40 and 46 2θ degrees, respectively. Note that all reflections on X-rays are characterized by significant widening, which is due to the nanodispersity of the material. The reflections of the platinum phase on X-ray diffractograms of commercial Pt/C catalysts are in the region of angles 2θ 39.9 and 45.6, which corresponds to the parameter of the platinum crystal lattice. At the same time, the reflections of Pt (111) and Pt (200) for all synthesized PtCo/C materials are shifted to the region of large values 2θ angles (Figure 2, curves 1.2), which indirectly indicates the formation of a platinum-cobalt solid solution [25–27,51]. Compositions of the metal component in PCC1 and PCC2 materials, calculated by extrapolating the dependence of the lattice parameter on the metal content in accordance with the Vegard's law as described in [52], turned out to be the—$Pt_{0.86}Co$ (Table 1).

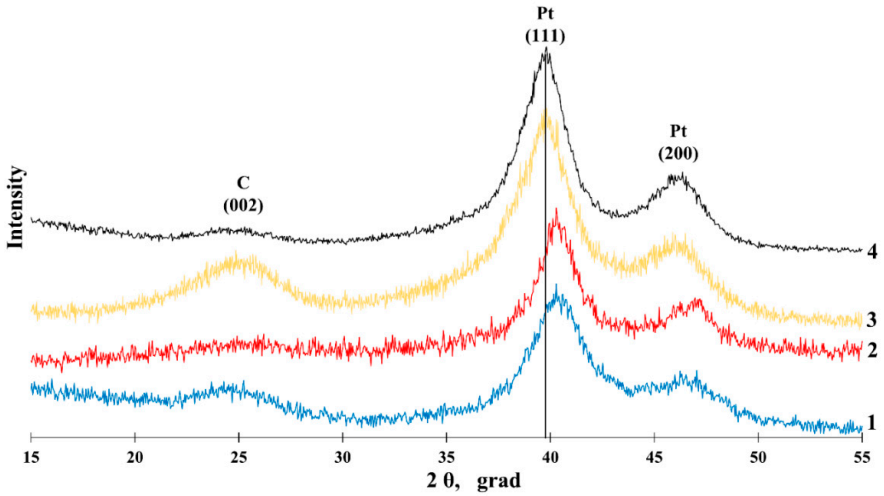

Figure 2. XRD patterns of PtCo/C materials: 1—PCC1; 2—PCC2; 3—commercial Pt/C sample (JM20); 4—commercial Pt/C sample (JM40).

The average crystallite size of PtCo nanoparticles calculated from the XRD (111) (see Experimental section) gave for PCC1and PCC2 values of 2.6 and 3.3 nm, respectively, which is slightly larger than the size of platinum crystallites in commercial catalysts JM20 and JM40 (Table 1). Despite the identity of the synthesis technique, an increase in the weight fraction of platinum from 14% (PCC1) to 30% (PCC2) has led to an increase in the average crystallite size—from 2.6 to 3.3 nm. Note that the PCC2 material is also close to the calculated composition value, determined from XRF and XRD data (Table 1).

The microstructure and composition of PCC1 and PCC2 materials were also studied by the TEM (Figure 3). On the micrographs of PCC1 material (Figure 3a,c) there is a large number of nanoparticles, with a diameter of 1.5 to 3.5 nm., as well as separate large agglomerates of nanoparticles. The average size of PtCo nanoparticles for PCC1 material

(3.0 nanometers) is slightly higher than the average crystallite size, determined from the XRD data. Sample PCC2 is characterized by a fairly narrow particle size distribution in the range of 3 to 5 nm (Figure 3f), but a large number of large agglomerates are observed. The average nanoparticle size (4.1 nm) is also slightly higher than the average crystallite size (3.0 nm) determined by the XRD. The situation, in which the average size of metal nanoparticles calculated from the TEM data is being slightly higher than the size calculated from the XRD, is typical of Pt/C and PtM/C materials and may be due to various reasons [31,53]. Comparing the morphology of synthesized PtCo/C materials and analogs described in the works of other authors, we note that a commercial PtCo/C catalyst with a more uniform distribution of PtCo nanoparticles over the surface of a carbon support is described by Moriau et al. [54]. However, the material considered by them contains larger particles and a significant amount of spherical agglomerates. Similar morphological features of PtCo/C catalysts are characteristic of a large number of studies [21,23,25,31,55].

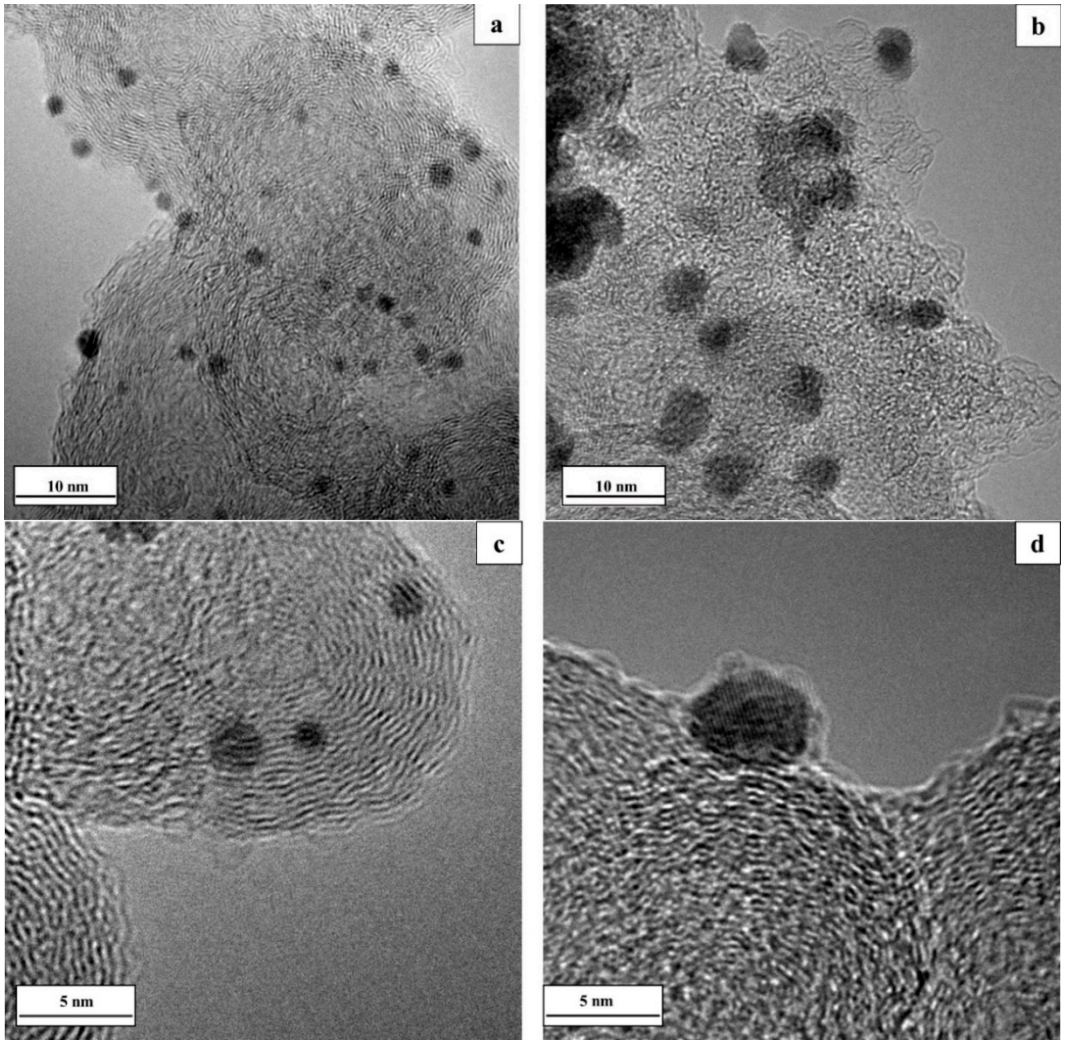

Figure 3. *Cont.*

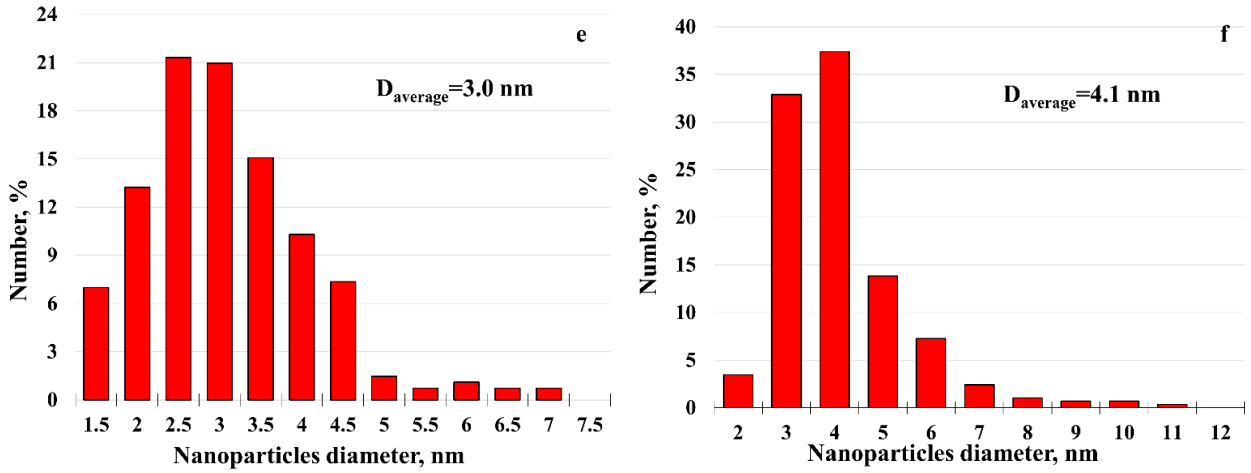

Figure 3. TEM images and histograms of the PtCo nanoparticles size distribution for PCC1 (**a**,**c**,**e**) and PCC2 (**b**,**d**,**f**).

The results of elemental mapping of the PCC1 and PCC2 materials surface fragments indicate the preferential localization of platinum and cobalt atoms in the same places (nanoparticles) (Figure 4), which also confirms the preferential formation of bimetallic nanoparticles as a result of synthesis. Determination of the test samples composition by the local EDAX microanalysis has given the atomic ratio of $PtCo_{1.05}$ and $PtCo_{1.27}$ for PCC1 and PCC2, respectively. These compositions are somewhat different from those determined by other methods of analysis (Table 1), but in general, they confirm the high content of cobalt in the materials obtained.

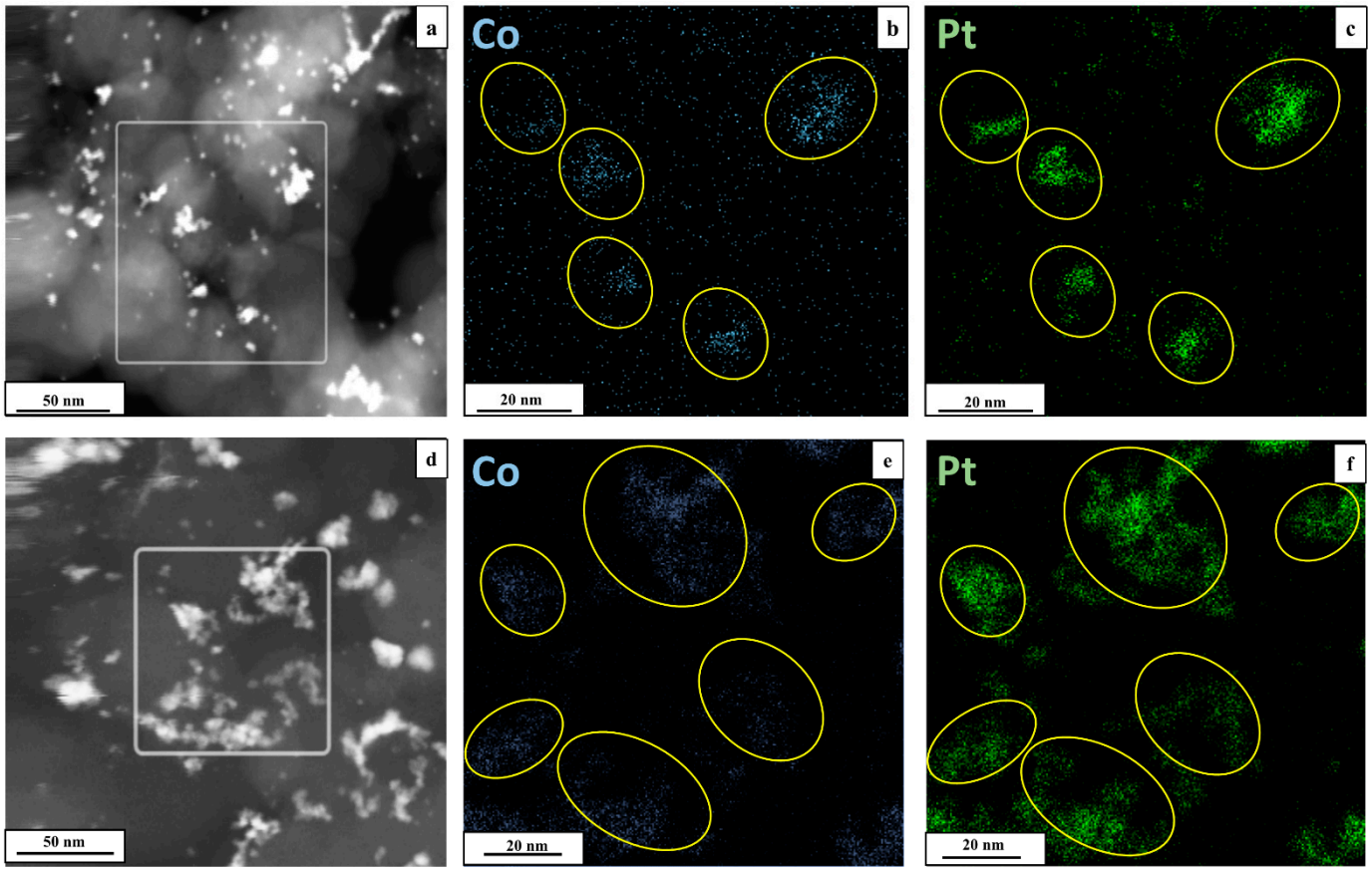

Figure 4. Elemental mapping of PtCo/C surface fragments for PCC1 (**a**–**c**) and PCC2 (**d**–**f**) samples.

Chemical state of platinum and cobalt, as well as compositions of PtCo/C and Pt/C catalysts were detected by the XPS. Typical X-ray photoelectron spectra of platinum ($Pt4f_{7/2}$) and cobalt ($Co2p_{3/2}$) for PtCo/C material are presented by PCC2 in Figure 5.

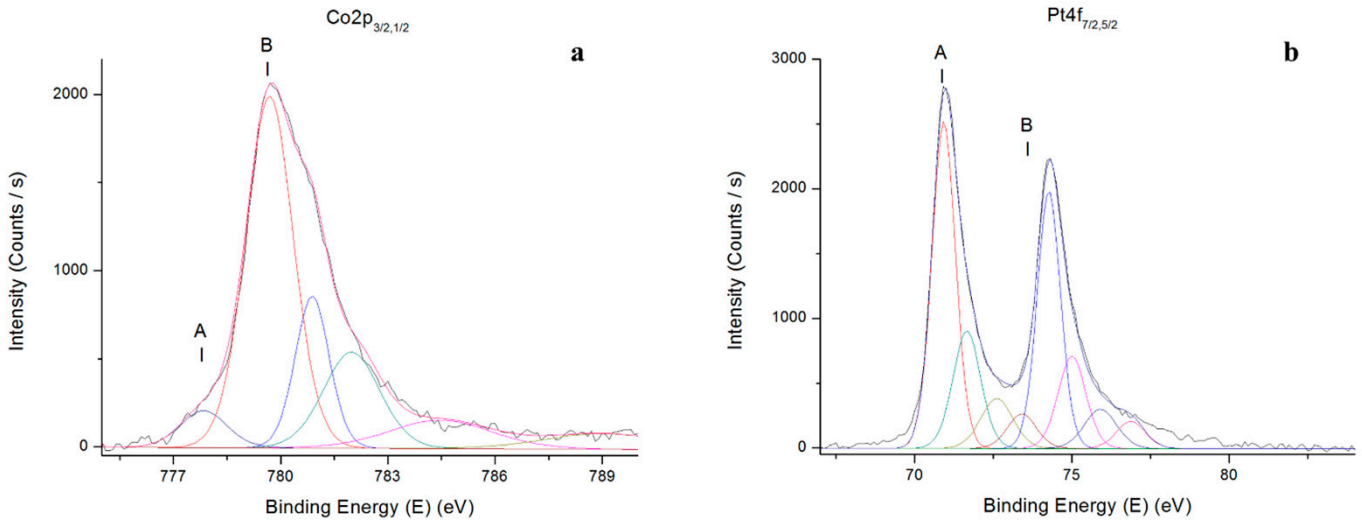

Figure 5. XPS spectra for (**a**) Co2p and (**b**) Pt4f of the PtCo/C catalyst PCC2.

Table 2 shows the binding energies of the $Pt4f_{7/2}$ and $Co2p_{3/2}$ spectra for both the PtCo/C samples and the commercial Pt/C catalyst. The binding energies of the components A of the $Pt4f_{7/2}$ spectra correspond to the metallic state of platinum atoms. The amount of PtO oxide (component B) does not exceed 5% for PtCo/C materials. The state of Co atoms in PtCo/C catalysts is directly opposite: cobalt is almost completely oxidized to the CoO state (component B of $Co2p_{3/2}$ spectra), and the amount of cobalt in the metallic state is about 6% (component A of $Co2p_{3/2}$ spectra). This result correlates with the data in [56], which showed that for Pt_3Co materials the cobalt content in the metallic state according to XPS data was 9.4%. Determination of the elemental composition of the studied samples by XPS demonstrated the atomic ratio $PtCo_{1.0}$ and $PtCo_{2.0}$ for PCC1 and PCC2, respectively. These compositions differ from those calculated by other analysis methods (Table 1), but indicate a higher cobalt content in PCC2 material, which is consistent with the results of other analysis methods. Note that the bond energies corresponding to the metallic platinum for the PtCo/C materials PCC 1 (70.96 eV) and PCC 2 (70.89 eV) are shifted to the region of high electron binding energy, compared to the commercial Pt/C material (70.84 eV) [57]. The results of XPS indicate the successful synthesis of PtCo bimetallic NPs on carbon support.

Table 2. Binding energies and the relative content of the Pt4f7/2 and Co2p3/2 components in the spectra of the studied samples.

Sample	$Pt4f_{7/2}$ A	$Pt4f_{7/2}$ B	$Co2p_{3/2}$ A	$Co2p_{3/2}$ B
JM-40	70.84 eV 94.2%	73.44 eV 5.8%	- 0.0%	- 0.0%
PCC2	70.89 eV 94.9%	73.42 eV 5.1%	777.8 eV 5.7%	779.6 eV 94.4%
PCC1	70.96 eV 95.1%	73.47 eV 4.9%	778.0 eV 6.5%	779.7 eV 93.5%

Thus, the results of the composition/microstructure study of the obtained PtCo/C materials taken as a whole, and the composition/structure of individual nanoparticles show that in the process of chemical reduction of Pt (IV) in solution, partial reduction of cobalt

oxides also occurs in composite CoO/C materials. As a result, bimetallic nanoparticles PtCo are formed on the surface/pores of the carbon support, and a part of the cobalt oxide remains unchanged.

Based on the results of the cyclic voltammetry (Figure 6), it was found that for synthesized PtCo/C samples, the values of specific currents per CV were significantly lower compared to currents for commercial JM20 and JM40 catalysts. Calculation of the ESA values for hydrogen adsorption/desorption showed that for the PCC1 catalyst the ESA value is 1.45 times less than the ESA of the commercial Pt/C sample JM20 (Table 3). Interestingly, an increase in the Pt weight fraction in PtCo/C samples did not lead to a decrease in the ESA. This positively distinguishes PCC series catalysts from commercial Pt/C materials, in which the ESA decreases from 74 to 48 m^2g^{-1} with an increase in the weight fraction of Pt from 20 to 40%. The values of specific currents for PCC2 and JM40 materials in the hydrogen adsorption/desorption region are close and, as a result, the ESA values of these catalysts are close (Figure 6).

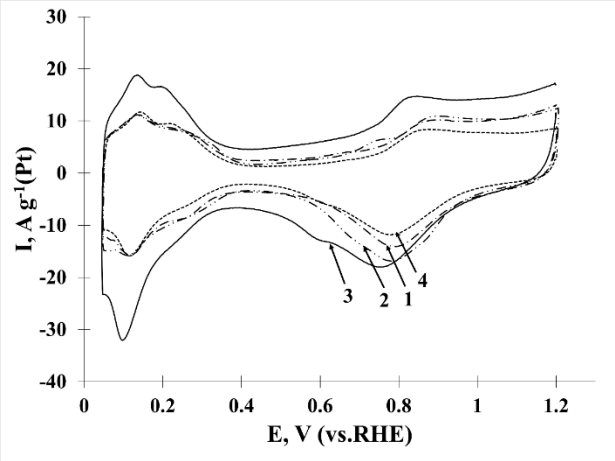

Figure 6. Cyclic voltammograms (2nd cycle). Electrolyte—1 M HClO4, Ar atmosphere. The scanning speed of the potential is 20 mVs−1: 1—PCC1; 2—PCC2; 3—Pt/C (JM20); 4—Pt/C (JM40).

Table 3. Parameters characterizing the electrochemical behavior of catalysts.

Sample	ESA		I_{mass}, Ag^{-1} (Pt) (E = 0.90 V)	I_s, Am^{-2} (Pt) (E = 0.90 V)	$E_{1/2}$	Number of ē (E = 0.90 V)
	$H_{ads/des}$ m^2g^{-1} (Pt)	CO m^2g^{-1} (Pt)				
PCC1	51 ± 5	58 ± 5	407 ± 20	8.0	0.92	4.1
PCC2	52 ± 5	45 ± 4	426 ± 21	8.9	0.94	4.0
JM20	74 ± 7	76 ± 7	220 ± 11	2.9	0.92	3.9
JM40	48 ± 5	51 ± 5	196 ± 10	4.1	0.92	3.8

Determination of the catalysts ESA by the method of oxidation of the chemosorbed CO monolayer (Figure 7, Table 3) for all catalysts showed a good correlation with the hydrogen adsorption/desorption data. The method of determining the area of materials by CO-stripping also provided additional information on the surface properties of metal nanoparticles. For this purpose, the onset values and maxima potentials of CO oxidation were compared. Note that bimetallic catalysts are characterized by several CO oxidation maxima as opposed to Pt/C catalysts (Figure 7). The presence of several maxima on CO oxidation voltammograms is quite common in various works [58–61]. This kind of CV can be related to the heterogeneity of the composition and structure of bimetallic nanoparticles [62,63] as well as the influence of different facets of platinum [61], or the presence of defects on the facets of platinum [64]. All these types of heterogeneity can be

characteristic of the PtCo/C materials we have obtained. Note that CO oxidation for both bimetallic catalysts begins at less positive potentials than for commercial Pt/C. The most intense peaks of CO oxidation on voltammograms of PtCo/C catalysts are also shifted towards smaller potentials. This indirectly indicates a lower susceptibility of the resulting bimetallic systems to CO poisoning and makes them very promising catalysts for organic oxidation reactions, in which CO is one of the intermediates [64]. It is known that positive shifts of the Pt 4f binding energies for PtCo/C catalyst, resulting from the changes of Pt electronic structures of Pt may have an effect on the activity of methanol oxidation [65].

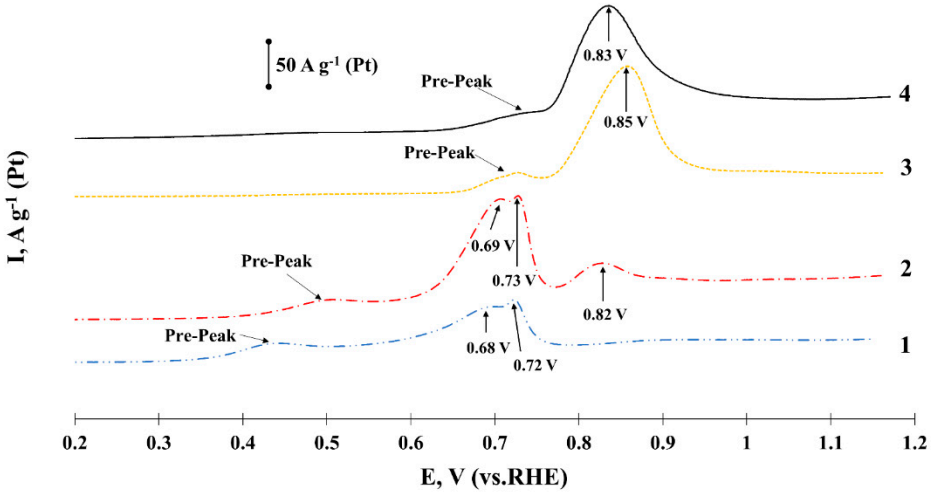

Figure 7. Cyclic voltammograms (2nd cycle). Electrolyte—1 M HClO4, Ar atmosphere. Potential sweep speed 40 mVs−1: 1—PCC1; 2—PC-2; 3—Pt/C (JM20); 4—Pt/C (JM40).

LSV measurements were carried out on the RDE in an oxygen-saturated electrolyte to assess catalyst activity in the ORR. Figure 8a shows typical liner sweep voltammograms for the oxygen reduction reaction on the PCC2 sample at different rotation speeds. Note that for all catalysts, the calculation of the number of electrons (z) involved in the ORR gave a value in the range of 3.8~4.1, which indicates a 4-electron mechanism of the ORR. In this case, the highest value of the half-wave potential is characteristic of the catalysts with a higher mass fraction of platinum in PCC2 and JM40. The results of voltammograms processing voltammograms in the Koutecký–Levich coordinates are shown in Figure 8b. For a bimetallic PtCo/C sample with a low mass fraction of Pt—PCC1, the mass activity is 53% higher compared to a commercial catalyst Pt/C containing 20% wt. The Pt sample PCC2 has the greatest activity among all studied catalysts. At close values of the ESA and average crystallite size (Table 1), the specific and mass activity of PCC2 is about 2 times higher than that of a 40% Pt/C catalyst JM40 (Table 3).

Note that the absolute mass activity values of the PtCo/C catalysts obtained in the present work are greater than those measured for the PtCo/C catalysts in [66,67]. Comparing our results with the literature data [25,55,68], we can conclude that the obtained PtCo/C catalysts are quite high in activity, their specific and mass activity of which significantly exceeds the activity of commercial Pt/C analogs. Stress testing of the catalysts leads to a decrease in their characteristics: the ESA value decreases, the half-wave potential shifts to the region of less positive values, and the activity in the ORR decreases (Figure 9a–f, Table 4). Changes in these characteristics can be used to compare durability of the catalysts.

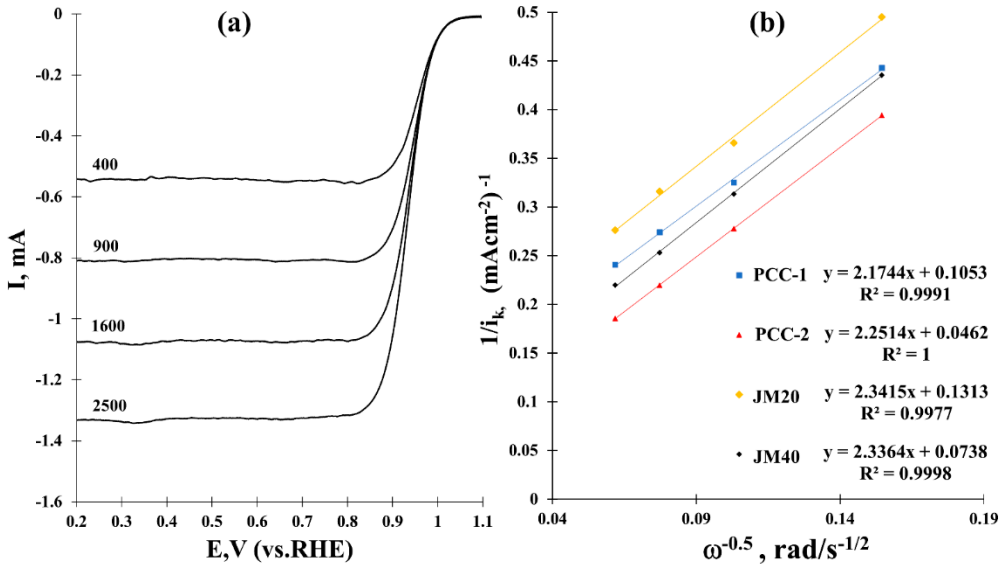

Figure 8. LSV curve for ORR at different rotation speeds (**a**) and the corresponding dependences $1/I_k$ vs. $\omega^{-1/2}$ at potential of 0.90 V. (**b**) Rotation speed 400, 900, 1600, 2500 rpm, potential sweep rate is 20 mVs^{-1}. Electrolyte—0.1 M $HClO_4$ solution saturated with O_2.

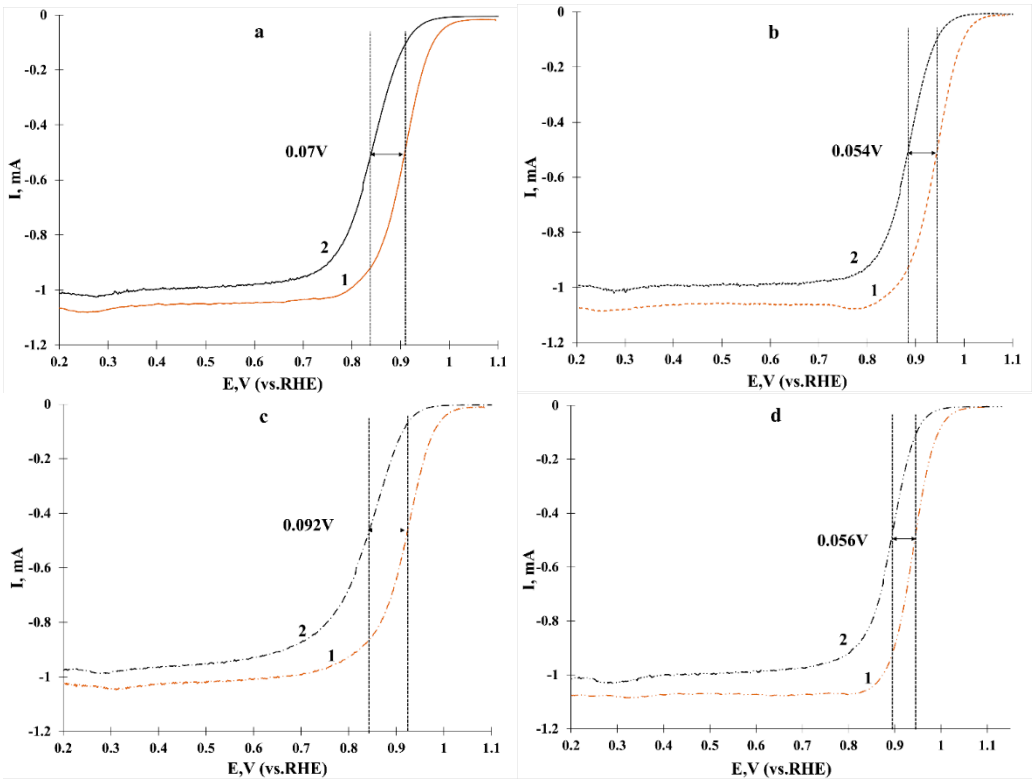

Figure 9. *Cont.*

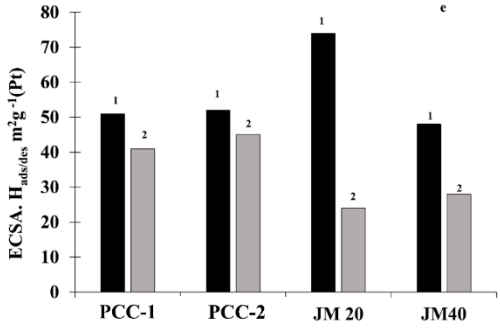

Figure 9. LSV curves for ORR before testing; 1 and 2—after stability tests (2000 cycles): (**a**)—commercial sample Pt/C (JM20); (**b**)—commercial sample Pt/C (JM40); (**c**)—sample PCC1; (**d**)—sample PC-2. Potential sweep speed—20 mVs−1, rotation speed—1600 rpm, 0.1 M HClO4, O2 atmosphere; (**e**)—histogram of ESA changes before test; 1 and 2—after test.

Table 4. Characteristics of catalysts on completion of voltammetric stress testing of 2000 cycles in the potential range of 0.6–1.4 V.

Sample	ESA $H_{ads/des}$ m^2g^{-1} (Pt)	I_{mass}, Ag^{-1} (Pt) (E = 0.85 V)	$E_{1/2}$
PCC1	41 ± 4	225 ± 11	0.85
PCC2	45 ± 4	466 ± 23	0.88
JM20	24 ± 2	145 ± 7	0.85
JM40	28 ± 3	246 ± 12	0.87

Taking into account changes in the ESA as a result of caused by stress testing (Tables 3 and 4, Figure 9e), the durability of catalysts is growing in the range: JM20 < < JM40 < < PCC1 ≤ PCC2. The value of half-wave potential grows in the series: JM20 ≈ PCC1 < JM40 < PCC2 (Figure 9a–d). Finally, according to the absolute values of mass activity in the ORR at E = 0.85 V after the stress test, a number of catalysts are as follows: JM20 < PCC1 ≤ JM40 < < PCC2. From the analysis of the above data, it can be concluded, that an increase in platinum loading in catalysts positively affects their durability: catalysts PCC2 and JM40 with 30–40% platinum loading are more stable than catalysts JM20 and PCC2 with 14–20% platinum loading; bimetallic catalyst PCC2 showed the highest durability in the stress test (according to the set of criteria). Note that the positive correlation between Pt-loading and catalyst durability has been demonstrated earlier, for example, in [69].

3. Experimental

3.1. Electrodeposition Technique

The synthesis of CoO_x/C composite materials was carried out by electrochemical deposition of cobalt onto a carbon support. The schematic representation of the electrochemical cell used for electrodeposition is shown in Figure 10a, a similar cell being used in [43]. The cathode was made in the form of a nickel plate (Figure 10a). The cathode surface was uniformly covered with a layer of a carbon paste, prepared for this particular purpose by dispersing 1 g of Vulcan XC-72 carbon (Cabot Corp.) for 1 min in 5 mL of glycerol (Vecton JSC). After that, the cell was carefully filled with an electrolyte, its composition being $CoSO_4 \times 7H_2O$ (Vecton JSC)—500g/L, NaCl (Vecton JSC)—15 g/L, H_3BO_3 (Vecton JSC)—45 g/L. A graphite anode was immersed in the electrolyte, followed by the electrodeposition process. When current was passed through the cell, the metal deposited on the surface of the carbon paste. At the same time, the surface of the carbon paste was constantly renewed due to diffusion and mixing, caused by the release of gaseous hydrogen (Figure 10b). Experimentally it was found that the time, at which the carbon paste layer was completely washed from the cathode surface, depended on the current regime. So,

with a 0.7A current, this process took about 15 min, and with a 1.4 A current only 4 min, due to a more intensive release of the gaseous hydrogen.

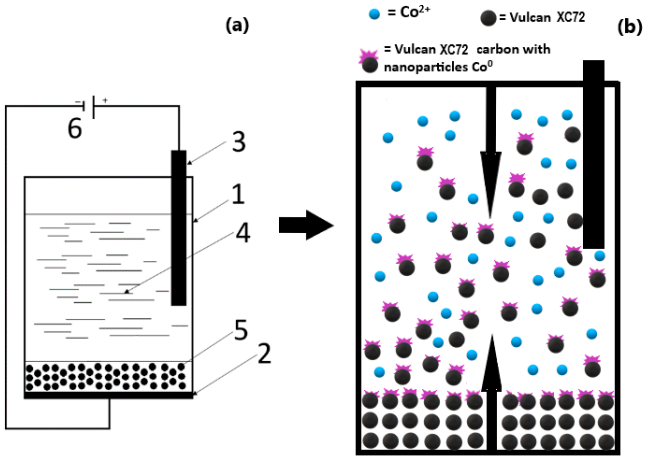

Figure 10. (**a**)—Electrical scheme of an electrodeposition CoO/C materials synthesis: 1—Teflon body, 2—nickel cathode, 3—graphite anode, 4—electrolyte, 5—layer of carbon paste, 6—direct current source. (**b**)—Pictorial description of a process of cobalt electrochemical deposition on carbon.

We failed in establishing a clear dependence of the oxide mass fraction deposited on carbon and the current mode. After electrodeposition, the suspension was filtered on a Buchner funnel through a blue tape filter, washed three times with deionized water and isopropyl alcohol, the filter with the material was placed in a petri dish, and left in a desiccator. While the Co/C material stayed in the electrolyte, being filtered and dried, there occurred the oxidation of metallic cobalt nanoparticles, which resulted in obtaining CoO_x/C (see Section 2) on completion of electrolysis. For the subsequent application of platinum, two samples of the composite CoO_x/C material were obtained with an oxide weight fraction of 8 wt% and 25 wt%, respectively, labeled as CC1 and CC2.

Platinum was applied to the resulting CoO_x/C composites by wet-synthesis using sodium borohydride (Vecton JSC) at room temperature. The calculated loading of platinum in $PtCoO_x$/C materials was 17 wt% and 32 wt%, respectively. The 0.15g CoO_x/C composite was placed in a mixture of 60 mL of ethylene glycol (EG) and 60 mL of bidistilled water, next the required amount of $H_2PtCl_6 \times 6H_2O$ (Aurat, Russia) was added as an aqueous solution. After ultrasonic homogenization of the suspension and 5-min stirring on a magnetic stirrer, a three-fold excess of $NaBH_4$ (Vecton JSC) in a 0.15 M aqueous solution was added uniformly dropwise over 1 min. $NaBH_4$ being added, the suspension was kept under stirring for 30 min. After synthesis, the suspension was filtered on a Buchner funnel through a blue tape filter, washed three times with deionized water and isopropyl alcohol, placed the filter with the material was placed in a petri dish, and left in a desiccator.

3.2. Measurement Methods and Techniques

To determine the amount of cobalt and platinum in the synthesized materials, a gravimetric analysis method was used: the mass of the substances remaining in the crucible after complete oxidation of carbon was determined by 30-min heating at 800 °C in an air atmosphere of 5–10 mg CoO_x/C or Pt/(CoO_x/C). Cobalt, when heated in a muffle furnace, formed Co_3O_4 oxide, so the results of thermogravimetry were converted to pure metal, taking into account oxide formation. The platinum-containing catalysts based on the CC1 and CC2 supports are further referred to as PCC1, PCC2.

The molar ratio of Pt:Co metals in the catalysts was determined by total reflection X-ray fluorescence analysis (XRF) on a spectrometer with a complete external reflection of X-ray radiation RFS-001 (Research Institute of Physics, SFedU, Rostov-on-Don, Russia). The exposure time of the samples was 300 s. The registration and processing of total reflection

X-ray fluorescent spectra was carried out using UniveRS software (Research Institute of Physics, SFedU, Rostov-on-Don, Russia). The content of the components was determined semi-quantitatively, relative to each other. For this, the integral areas under the peaks corresponding to Pt and Co were calculated. Note that this method does not identify the state of the metal in the sample (atomic, ionic). The error of the XRF method in determining the composition was $PtCo_{x\pm0.02}$.

X-ray phase analysis (XRD) was used to determine the phase composition of the samples and the size of the nanoparticles (crystallites). XRD patterns were recorded on an ARL X'TRA diffractometer with Breggu-Brentano geometry. Typical settings: 40 kW, 35 mA, scanning step 0.02 degrees in coordinates 2θ, shooting speed 2 degrees per minute. Phase analysis was carried out on the basis of the data obtained from the open sources, Crystallography Open Database (COD) being also used [70,71]. The fitting of the X-ray patterns was carried out using a SciDavIs processing packet, the position of the peaks, their full width at half maximum (FWHM) and area were determined by the Lorentz function approximation method. The average size of platinum or alloys crystallites thereof was determined by diffractograms using reflection (111). The average crystallite diameter was determined by the Scherrer formula (1) as described in [72], in which the corresponding value of the full width at half maximum (FWHM) was substituted:

$$D_{hkl} = K \times \lambda / [FWHM \times \cos(\theta)] \quad (1)$$

where λ—is the wavelength of monochromatic radiation; FWHM—full width at half maximum (in radians); D_{hkl} is the average thickness of the "stack" of reflecting planes in the coherent scattering region, i.e., the average diameter of the crystallites; θ—the angle of reflection; K = 0.89—the Scherrer constant. To take instrumental widening into account, the diffractometer was pre-calibrated using a plate of polycrystalline annealed α-quartz with a grain size of 2 to 4 microns as a standard sample.

Transmission electron microscopy (TEM) analysis of the catalysts composition and microstructure was carried out on microscopes JEM-2100 (JEOL, Japan) and FEI Tecnai G2 F20S-TWIN TMP with an EDAX module, operating at an accelerating voltage of 200 kW. Electrocatalyst powders (0.5 mg) were placed in 1 mL of heptane to prepare samples for TEM analysis. The suspension was then dispersed by ultrasound, next a drop of suspension was applied to a copper mesh, coated with a thin layer of amorphous carbon. The elemental composition analysis was carried out by identifying the X-ray signal obtained at a certain position point (region) from the energy scale of the characteristic lines of the elements, which were compared with the tabular data. Further on, using the eZAF (MThin) program algorithm implemented in the «EDAX TEAM» software, element concentrations were calculated, their peak intensity and secondary X-ray output section for the lines of each element at each point of the map being taken into account. The presence/absence of the secondary phases and their elemental composition was carried out according to the EMF mapping data by analyzing the difference in concentrations in individual zones on the EMF map. X-ray photoelectron spectroscopy (XPS) was obtained on the X-ray photoelectron spectrometer ESCALAB 250 using a monochromatized Al K_a X-ray line with an energy of 1486.6 eV. The minimum allowable energy range determined by the doublet Ag $3d_{5/2,3/2}$ did not exceed 0.6 eV. Powdered samples were applied to Carbon Tape, which was attached to a standard spectrometer sample holder. The spectra were processed using Avantage™ software. As part of the processing of the spectra, the background was subtracted using the Smart form, the XPS lines were approximated by L/G Mix functions (30% Lorencian, 70% Gaussian). To approximate (fitting) asymmetric XPS lines of 3d (Co) and 5d (Pt) metals when using the Avantage software, was used, in addition to the main component (Co2p3 A and Pt4f7 A), 2–3 additional components (B, C, etc.) to compensate for the asymmetry of the corresponding line. The main information about the chemical bond is carried by component A of the spectra (its so-called bond energy). Other components' contribution to the total line intensity is taken into account when calculating the elemental composition.

Cyclic voltammetry (CV) was used to determine the area of the electrochemical active surface (ESA) of platinum. A thin (about 4 μm) layer of the test material was applied to the glass carbon end of the rotating disk electrode. To form a thin layer of the material under study, 6 μL of the suspension was applied to the end face of a glass-graphite rotating disk electrode (VDE). The suspension had the following catalyst composition in a water—isopropanol mixture containing the addition of Nafion polymer and 0.6 μg of catalyst. After drying, another 7 μL of 0.05% Nafion solution was applied to fix the layer, after that the electrode was dried for 5 min at room temperature. Using potentiostat VersaSTAT 3 (AMETEK Scientific Instruments, USA), a potential sweep was set, and current values were fixed. Initially, to standardize the surface of Pt and completely remove impurities, 100 cycles of potential scanning were carried out at a rate of 200 mV s^{-1} in the range of potentials from 0.05 to 1.2 V (relative to RHE). Then, 2 cyclic voltammograms (CV) were recorded in the range of potentials 0.05–1.2 V at a scanning rate of 20 mV s^{-1}. The amount of electricity was calculated on the "hydrogen" areas of the CV in the current-time coordinates using the VersaStudio software. That was ensured by averaging the amount of electricity spent on electrochemical adsorption and hydrogen desorption on platinum, the amount of electricity spent on charging the double electric layer being subtracted. All measurements were performed at room temperature. Calculation of the electrochemical active surface area was carried out according to the formula:

$$\mathrm{ESA} = \frac{\mathrm{Q}}{\mathrm{m} \times 210},\ \mathrm{cm^2 g^{-1}(Pt)} \quad (2)$$

where Q is the average value (half-sum) of the amounts of electricity (μC) spent on electrochemical adsorption and desorption of hydrogen; m is the mass of platinum on the electrode (g);

210 (μCcm^{-2}) is the amount of electricity required for electrochemical adsorption or desorption of a monolayer of atomic hydrogen from 1 cm^2 of platinum surface.

The active surface area of the metals was also determined by the amount of electrochemically oxidized chemosorbed CO (CO-stripping). To this end, while maintaining a constant electrode potential of 0.1 V, CO was blown through the electrolyte for 30 min, and then argon—for 30 min. Next, a cyclic voltammograms (CVs) (3 cycles) were recorded in the range of potentials from 0.05 to 1.20 V with a potential sweep rate of 20 mVs^{-1}. The ESA value was calculated from the amount of electricity spent in the first cycle on CO oxidation, chemosorbed on the surface of metals.

When the ESA of the materials was determined, their activity in ORR was examined at the rotational speeds of the disk electrode: 400, 900, 1600 and 2500 revolutions per minute (rpm). Linear sweep voltammograms (LSV) were previously recorded in an argon atmosphere to further "subtract" them from LSV, obtained in an oxygen atmosphere: $I = I_{O2} - I_{Ar}$. This allowed us to take into account the influence of background currents. Measurements were carried out in a standard three-electrode cell using 0.1M $HClO_4$ (Vekton Ltd.) as a background electrolyte. Prior to the measurements, the working solution was purged with O_2 for 40 min at atmospheric pressure. Voltammograms were recorded in the direction from 0.02 V to 1.20 V at a potential scanning rate of 20 m$V{\cdot}s^{-1}$. Then, the dependence of the current value on the rotation speed of the disk electrode was analyzed using the Koutecký–Levich equation, which allows separating the kinetic and diffusion components of the current:

$$\frac{1}{i} = \frac{1}{i_k} + \frac{1}{i_\partial} = \frac{1}{i_k} + \frac{1}{Bz\omega^{0.5}},\ \text{where } B = 0.62{\cdot}F{\cdot}D^{2/3}{\cdot}\nu^{-1/6}{\cdot}c \quad (3)$$

z—the number of electrons carried during electric reduction of the molecule O_2; F—Faraday's number; D—coefficient of oxygen diffusion; ν—kinematic viscosity; ω—the rotation speed of the electrode; c—the concentration of reacting particles (oxygen molecules) in the solution.

The measurements were adjusted for the system ohmic resistance (R = 26 ohms) as described in [73]. Since the absolute values of the ESA and catalyst activity in electrochemical reactions were very sensitive to the structure of the catalyst bed and the purity of the electrolyte, commercial Pt/C catalysts of HiSPEC3000 (Johnson Matthey) containing 20 wt% Pt and HiSPEC4000 (Johnson Matthey) containing 40 wt% Pt were used as standard samples. The composition of the catalytic ink and the method of applying the catalyst layer for HiSPEC3000 and HiSPEC4000 were the same as for the catalysts under study. A silver chloride electrode was used as the reference electrode. All potential values in the operation were given relative to the potential of a reversible hydrogen electrode (RHE).

Stability assessment was carried out by voltammetric cycling in a three-electrode cell in the range of potentials 0.6–1.4 V with a scanning rate of 100 mVs^{-1}. Cycling was carried out in 0.1 M $HClO_4$ solution under Ar atmosphere at 25 °C for 2000 cycles. After each 100 cycles, two cyclic voltammograms were recorded (at a potential scanning rate of 20 mVs^{-1}, potential range of 0.05 to 1.20 V). The second CV was calculated as described above. Stability was evaluated both by changing the absolute values of the ESA and by changing the ratio of the ESA/ESA_0, where j is the number of stress test cycles performed (ESA_{2000}/ESA_0).

4. Conclusions

By electrochemical deposition of cobalt onto carbon support particles at direct current, CoO_x/C composite support containing 8 and 25 wt% cobalt oxide were successfully obtained. By the chemical reduction of platinum from H_2PtCl_6 solutions, using sodium borohydride on the basis of the obtained CoO_x/C composite supports, $PtCoO_x/C$ catalysts of $Pt_{1.56}Co$ and $Pt_{1.12}Co$ composition containing 14 and 30 wt% Pt, respectively, were synthesized. The resulting bimetallic catalysts have a small average crystallite size of 2.6 to 3.3 nm according to the XRD data and a small average nanoparticle size according to the TEM data of 3.0 to 4.1 nm. Based on the XRD and the TEM with EDX mapping, we can make a conclusion of the preferential formation of bimetallic Pt-Co nanoparticles.

On the other hand, the XPS data, comparison of the materials composition performed according to the XRF and a calculation according to the Vegard law make it possible to conclude that a certain part of cobalt is not included in the content of bimetallic nanoparticles and is contained in the form of the X-ray amorphous oxide.

The obtained PtCo/C materials show up to 2 times the specific catalytic activity in the ORR compared to commercial Pt/C analogs. According to the results of the accelerated stress test, PtCo/C materials showed greater stability compared to Pt/C analogs. On the basis set of these characteristics, the bimetallic PCC2 catalyst with the $Pt_{1.12}Co$ structure has demonstrated the highest activity in the ORR and durability in a stress test among all studied materials. We believe that the electrolytic technique of gram-scale synthesis of the composite CoO_x/C carriers described in the paper can be used in the large-scale production of PtCo/C electrocatalysts.

Author Contributions: Conceptualization, V.G. and S.B.; methodology, D.M.; validation, D.M., A.N. (Alexey Nikulin) and A.N. (Anatoly Nikolsky); formal analysis, D.A. and A.K.; investigation, D.M.; data curation, D.M., A.N. (Alexey Nikulin), V.G. and S.B.; writing—original draft preparation, D.M.; writing—review and editing, V.G., S.B. and O.S.; visualization, D.M. and S.B.; supervision, V.G. and S.B.; project administration, V.G. All authors have read and agreed to the published version of the manuscript.

Funding: This research was financially supported by the Ministry of Science and Higher Education of the Russian Federation (State assignment in the field of scientific activity No 0852-2020-0019).

Data Availability Statement: The data presented in this study is available upon request from the respective author. The data is not publicly available due to the planned preparation of the patent.

Acknowledgments: The authors are grateful to Alekseenko A.A. for helpful suggestions for making improvements in the present article and appreciate the support by LLC "PROMETHEUS R&D"

(Rostov-on-Don) and LLC "Systems for Microscopy and Analysis" (Skolkovo, Moscow) for conducting TEM and EDX studies.

Conflicts of Interest: The authors declare no conflict of interest.

Abbreviations

CV	Cyclic voltammogram
ESA	Electrometrically active surface area
LSV	Linear sweep voltammetry
ORR	Oxygen reduction reaction
RDE	Rotating disk electrode
RHE	Reversible hydrogen electrode
XRD	X-ray diffraction
XRF	X-ray fluorescence analysis
XPS	X-ray photoelectron spectroscopy
TEM	Transmission electron microscopy

References

1. Pettersson, J.; Ramsey, B.; Harrison, D. A review of the latest developments in electrodes for unitised regenerative polymer electrolyte fuel cells. *J. Power Sources* **2006**, *157*, 28–34. [CrossRef]
2. Alaswad, A.; Baroutaji, A.; Achour, H.; Carton, J.; Al Makky, A.; Olabi, A.G. Developments in fuel cell technologies in the transport sector. *Int. J. Hydrogen Energy* **2016**, *41*, 16499–16508. [CrossRef]
3. Nørskov, J.K.; Rossmeisl, J.; Logadottir, A.; Lindqvist, L.; Kitchin, J.R.; Bligaard, T.; Jónsson, H. Origin of the Overpotential for Oxygen Reduction at a Fuel-Cell Cathode. *J. Phys. Chem. B* **2004**, *108*, 17886–17892. [CrossRef]
4. Filippov, S.P.; Yaroslavtsev, A.B. Hydrogen energy: Development prospects and materials. *Russ. Chem. Rev.* **2021**, *90*, 627–643. [CrossRef]
5. Gomez-Marin, A.M.; Rizo, R.; Feliu, J.M. Oxygen reduction reaction at Pt single crystals: A critical overview. *Catal. Sci. Technol.* **2014**, *4*, 1685–1698. [CrossRef]
6. Sorsa, O.; Romar, H.; Lassi, U.; Kallio, T. Co-electrodeposited mesoporous PtM (M=Co, Ni, Cu) as an active catalyst for oxygen reduction reaction in a polymer electrolyte membrane fuel cell. *Electrochim. Acta.* **2017**, *230*, 49–57. [CrossRef]
7. Mohl, M.; Dobo, D.; Kukovecz, A.; Konya, Z.; Kordas, K.; Wei, J.; Vajtai, R.; Ajayan, P.M. Formation of CuPd and CuPt Bimetallic Nanotubes by Galvanic Replacement Reaction. *J. Phys. Chem. C* **2011**, *115*, 9403–9409. [CrossRef]
8. Asset, T.; Chattot, R.; Fontana, M.; Mercier-Guyon, B.; Job, N.; Dubau, L.; Maillard, F. A Review on Recent Developments and Prospects for the Oxygen Reduction Reaction on Hollow Pt-alloy Nanoparticles. *ChemPhysChem* **2018**, *19*, 1552–1567. [CrossRef]
9. Antolini, E. Formation of carbon-supported PtM alloys for low temperature fuel cells: A review. *Mater. Chem. Phys.* **2003**, *78*, 563–573. [CrossRef]
10. Jalan, V.M.; Taylor, E.J. Importance of Interatomic Spacing in Catalytic Reduction of Oxygen in Phosphoric Acid. *J. Electrochem. Soc.* **1983**, *130*, 2299–2302. [CrossRef]
11. Toda, T.; Igarashi, H.; Uchida, H.; Watanabe, M. Enhancement of the Electroreduction of Oxygen on Pt Alloys with Fe, Ni, and Co. *J. Electrochem. Soc.* **1999**, *146*, 3750–3756. [CrossRef]
12. Munoz, M.; Ponce, S.; Zhang, G.R.; Etzold, B.J.M. Size-controlled PtNi nanoparticles as highly efficient catalyst for hydrodechlorination reactions. *Appl. Catal. B Environ.* **2016**, *192*, 1–7. [CrossRef]
13. Beard, B.C.; Ross, P.N. The Structure and Activity of Pt-Co Alloys as Oxygen Reduction Electrocatalysts. *J. Electrochem. Soc.* **1990**, *137*, 3368–3374. [CrossRef]
14. He, C.; Zhang, S.; Tao, J.; Shen, P.K. One-step solid state synthesis of PtCo nanocubes graphene nanocomposites as advanced oxygen reduction reaction electrocatalysts. *J. Catal.* **2018**, *362*, 85–93. [CrossRef]
15. Stamenkovic, V.; Schmidt, T.J.; Ross, P.N.; Markovic, N.M. Surface Composition Effects in Electrocatalysis: Kinetics of Oxygen Reduction on Well-Defined Pt3Ni and Pt3Co Alloy Surfaces. *J. Phys. Chem.* **2002**, *106*, 11970–11979. [CrossRef]
16. Konno, N.; Mizuno, S.; Nakaji, H.; Ishikawa, Y. Development of compact and high-performance fuel cell stack. *SAE Int. J. Altern. Powertains* **2015**, *4*, 123–129. [CrossRef]
17. Zhang, X.F.; Zhu, X.Y.; Feng, J.J.; Wang, A.J. Solvothermal synthesis of N-doped graphene supported PtCo nanodendrites with highly catalytic activity for 4-nitrophenol reduction. *Appl. Surf. Sci.* **2018**, *428*, 798–808. [CrossRef]
18. Meng, H.B.; Zhang, X.F.; Pu, Y.L.; Chen, X.L.; Feng, J.J.; Han, D.M.; Wang, A.J. One-pot solvothermal synthesis of reduced graphene oxide-supported uniform PtCo nanocrystals for efficient and robust electrocatalysis. *J. Colloid Interface Sci.* **2019**, *543*, 17–24. [CrossRef]
19. Hu, S.; Wang, Z.; Chen, H.; Wang, S.; Li, X.; Zhang, X.; Shen, P.K. Ultrathin PtCo nanorod assemblies with self-optimized surface for oxygen reduction reaction. *J. Electroanal. Chem.* **2020**, *870*, 114194–114201. [CrossRef]

20. Stamenkovic, V.; Mun, B.S.; Mayrhofer, K.J.J.; Ross, P.N.; Markovic, N.M.; Rossmeisl, J.; Greeley, J.; Nørskov, J.K. Changing the activity of electrocatalysts for oxygen reduction by tuning the surface electronic structure. *Angew. Chem. Int. Ed.* **2006**, *45*, 2897–2901. [CrossRef]
21. Grolleau, C.; Coutanceau, C.; Pierre, F.; Leger, J.M. Optimization of a surfactant free polyol method for the synthesis of platinum–cobalt electrocatalysts using Taguchi design of experiments. *J. Power Sources* **2010**, *195*, 1569–1576. [CrossRef]
22. Miyatake, K.; Shimizu, Y. Pt/Co Alloy Nanoparticles Prepared by Nanocapsule Method Exhibit a High Oxygen Reduction Reaction Activity in the Alkaline Media. *ACS Omega* **2017**, *2*, 2085–2089. [CrossRef]
23. Cai, Y.Z.; Gao, P.; Wang, F.H.; Zhu, H. Carbon supported chemically ordered nanoparicles with stable Pt shell and their superior catalysis toward the oxygen reduction reaction. *Electrochim. Acta* **2017**, *245*, 924–933. [CrossRef]
24. Zhang, S.; Jiang, B.; Jiang, K.; Cai, W.B. Surfactant-Free Synthesis of Carbon-Supported Palladium Nanoparticles and Size-Dependent Hydrogen Production from Formic Acid–Formate Solution. *ACS Appl. Mater. Interfaces* **2017**, *9*, 24678–24687. [CrossRef] [PubMed]
25. Huang, J.; Ding, C.; Yang, Y.; Liu, G.; Cai, W.B. An alternate aqueous phase synthesis of the Pt_3Co/C catalyst towards efficient oxygen reduction reaction. *Chin. J. Catal.* **2019**, *40*, 1895–1903. [CrossRef]
26. Antolini, E.; Salgado, J.; Giz, M.; Gonzalez, E. Effects of geometric and electronic factors on ORR activity of carbon supported Pt–Co electrocatalysts in PEM fuel cells. *Int. J. Hydrogen Energy* **2005**, *30*, 1213–1220. [CrossRef]
27. Jiang, R.; Rong, C.; Chu, D. Surface coverage of Pt atoms on PtCo nanoparticles and catalytic kinetics for oxygen reduction. *Electrochim. Acta* **2011**, *56*, 2532–2540. [CrossRef]
28. Hernández-Fernández, P.; Rojas, S.; Ocón, P.; de la Fuente, J.L.G.; Terreros, P.; Peña, M.A.; García-Fierro, J.L. An opening route to the design of cathode materials for fuel cells based on PtCo nanoparticles. *Appl. Catal. B Environ.* **2007**, *77*, 19–28. [CrossRef]
29. Koh, S.; Toney, M.F.; Strasser, P. Activity–stability relationships of ordered and disordered alloy phases of Pt3Co electrocatalysts for the oxygen reduction reaction (ORR). *Electrochim. Acta* **2007**, *52*, 2765–2774. [CrossRef]
30. Hou, F.; Zhao, H.; Song, H.; Chou, L.; Zhao, J.; Yang, J.; Yan, L. Effect of impregnation strategy on catalytic hydrogenation behavior of PtCo catalysts supported on $La_2O_2CO_3$ nanorods. *J. Rare Earths* **2018**, *36*, 965–973. [CrossRef]
31. Mondal, A.; De, A.; Datta, J. Selective methodology for developing PtCo NPs and performance screening for energy efficient electro-catalysis in direct ethanol fuel cell. *J. Int. J. Hydrogen Energy* **2019**, *44*, 10996–11011. [CrossRef]
32. Choi, J.; Jang, J.H.; Roh, C.W.; Yang, S.; Kim, J.; Lim, J.; Lee, H. Gram-scale synthesis of highly active and durable octahedral PtNi nanoparticle catalysts for proton exchange membrane fuel cell. *Appl. Catal. B Environ.* **2018**, *225*, 530–537. [CrossRef]
33. Lim, I.; Lee, E.; Park, H.U.; Jang, J.; Jung, N.; Yang, T.H.; Park, G.G. Sonochemical gram-scale synthesis of core–shell PdCo@Pt nanoparticle and investigation of post heat-treatment effect for various gas atmospheres. *J. Alloys Compd.* **2021**, *879*, 160441. [CrossRef]
34. Poly, S.S.; Hashiguchi, Y.; Sultana, A.; Nakamura, I.; Shimizu, K.; Yasumura, S.; Fujitani, T. Flow reactor approach for the facile and continuous synthesis of efficient Pd@Pt core-shell nanoparticles for acceptorless dehydrogenative synthesis of pyrimidines from alcohols and amidines. *Appl. Catal. A Gen.* **2021**, *619*, 118158. [CrossRef]
35. Lin, R.; Cai, X.; Hao, Z.; Pu, H.; Yan, H. Rapid microwave-assisted solvothermal synthesis of shape-controlled Pt-Ni alloy nanoparticles for PEMFC. *Electrochim. Acta* **2018**, *283*, 764–771. [CrossRef]
36. Domynguez-Domynguez, S.; Arias-Pardilla, J.; Berenguer-Murcia, Á.; Morallyn, E.; Cazorla-Amorys, D. Electrochemical deposition of platinum nanoparticles on different carbon supports and conducting polymers. *J. Appl. Electrochem.* **2008**, *38*, 259–268. [CrossRef]
37. Feng, J.J.; Li, A.Q.; Wang, A.J.; Lei, Z.; Chen, J.R. Electrodeposition of monodispersed platinum nanoparticles on a glassy carbon electrode for sensing methanol. *Microchim. Acta* **2011**, *173*, 383–389. [CrossRef]
38. Tang, H.; Chen, J.H.; Huang, Z.P.; Wang, D.Z.; Ren, Z.F.; Nie, L.H.; Kuang, Y.F.; Yao, S.Z. High dispersion and electrocatalytic properties of platinum on well-aligned carbon nanotube arrays. *Carbon* **2004**, *42*, 191–197. [CrossRef]
39. Zhang, L.; Fang, Z.; Zhao, G.C.; Wei, X.W. Electrodeposited platinum nanoparticles on the multi-walled carbon nanotubes and its electrocatalytic for nitric oxide. *Int. J. Electrochem. Sci.* **2008**, *3*, 746–754.
40. Wei, Z.D.; Chan, S.H.; Li, L.L.; Cai, H.F.; Xia, Z.T.; Sun, C.X. Electrodepositing Pt on a Nafion-bonded carbon electrode as a catalyzed electrode for oxygen reduction reaction. *Electrochim. Acta* **2005**, *50*, 2279–2287. [CrossRef]
41. Santiago, D.; Rodryguez-Calero, G.G.; Rivera, H.; Tryk, D.A.; Scibioh, M.A. Cabrera CR Platinum electrodeposition at high surface area carbon Vulcan XC-72 material using a rotating disk -slurry electrode technique. *J. Electrochem. Soc.* **2010**, *157*, F189–F195. [CrossRef]
42. Chaisubanan, N.; Tantavichet, N. Pulse reverse electrodeposition of Pt–Co alloys onto carbon cloth electrodes. *J. Alloys Compd.* **2013**, *559*, 69–75. [CrossRef]
43. Burk, J.J.; Buratto, S.K. Electrodeposition of Pt Nanoparticle Catalysts from $H_2Pt(OH)_6$ and Their Application in PEM Fuel Cells. *J. Phys. Chem. C* **2013**, *117*, 18957–18966. [CrossRef]
44. Sieben, J.M.; Morallón, E.; Cazorla-Amorós, D. Flexible ruthenium oxide-activated carbon cloth composites prepared by simple electrodeposition methods. *Energy* **2013**, *58*, 519–526. [CrossRef]
45. Novomlinski, I.N.; Tabachkova, N.Y.; Safronenko, O.I.; Guterman, V.E. A novel electrochemical method for the preparation of Pt/C nanostructured materials. *Mon. Für Chem. Chem. Mon.* **2019**, *150*, 631–637. [CrossRef]

46. Kuriganova, A.B.; Leontyeva, D.V.; Ivanov, S.; Bund, A.; Smirnova, N.V. Electrochemical dispersion technique for preparation of hybrid MOx–C supports and Pt/MOx–C electrocatalysts for low temperature fuel cells. *J. Appl. Electrochem.* **2016**, *46*, 1245–1260. [CrossRef]
47. Guterman, V.E.; Novomlinskij, I.N.; Skibina, L.M.; Mauer, D.K. Method for Obtaining Nanostructural Material of Tin Oxide on Basis of Carbon. Invention Patent RUS 2656914, 7 June 2018.
48. Mauer, D.K.; Belenov, S.V.; Skibina, L.M.; Guterman, V.E. Composite Pt/(SnO_2/C) and PtSnNi/C Catalysts for Oxygen Reduction and Alcohol Electrooxidation Reaction. *Russ. J. Electrochem.* **2021**, *57*, 898–910. [CrossRef]
49. Novomlinskiy, I.N.; Danilenko, M.V.; Safronenko, O.I.; Tabachkova, N.Y.; Guterman, V.E. Influence of the Sn-Oxide-Carbon Carrier Composition on the Functional Characteristics of Deposited Platinum Electrocatalysts. *Electrocatalysis* **2021**, *12*, 489–498. [CrossRef]
50. Menshchikov, V.S.; Belenov, S.V.; Guterman, V.E.; Novomlinskiy, I.N.; Nevel'skaya, A.K.; Nikulin, A.Y. Methanol Electrooxidation on PtM/C (M = Ni, Co) and Pt/(SnO_2/C) Catalysts. *Russ. J. Electrochem.* **2018**, *54*, 937–948. [CrossRef]
51. Travitsky, N.; Ripenbein, T.; Golodnitsky, D.; Rosenberg, Y.; Burshtein, L.; Peled, E. Pt-, PtNi- and PtCo-supported catalysts for oxygen reduction in PEM fuel cells. *J. Power Sources* **2006**, *161*, 782–789. [CrossRef]
52. Denton, A.R.; Ashcroft, N.W. Vegard's law. *Phys. Rev. A* **1991**, *43*, 3161–3164. [CrossRef]
53. Favilla, P.C.; Acosta, J.J.; Schvezov, C.E.; Sercovich, D.J.; Collet-Lacos, J.R. Size control of carbon-supported platinum nanoparticles made using polyol method for low temperature fuel cells. *Chem. Eng. Sci.* **2013**, *101*, 27–34. [CrossRef]
54. Moriau, L.J.; Hrnjic, A.; Pavlisic, A.; Kamsek, A.R.; Petek, U.; Ruiz-Zepeda, F.; Sala, M.; Pavko, L.; Selih, V.S.; Bele, M.; et al. Resolving the nanoparticles' structure-property relationships at the atomic level: A study of Pt-based electrocatalysts. *iScience* **2021**, *24*, 102102. [CrossRef] [PubMed]
55. Li, B.; Yan, Z.; Xiao, Q.; Dai, J.; Yang, D.; Zhang, C.; Cai, M.; Ma, J. Highly active carbon-supported Pt nanoparticles modified and dealloyed with Co for the oxygen reduction reaction. *J. Power Sources* **2014**, *270*, 201–207. [CrossRef]
56. García-Contreras, M.A.; Fernández-Valverde, S.M.; Vargas-García, J.R.; Cortés-Jácome, M.A.; Toledo-Antonio, J.A.; Ángeles-Chavez, C. Pt, PtCo and PtNi electrocatalysts prepared by mechanical alloying for the oxygen reduction reaction in 0.5 M H_2SO_4. *Int. J. Hydrogen Energy* **2008**, *33*, 6672–6680. [CrossRef]
57. Zhang, Z.C.; Tian, X.C.; Zhang, B.W.; Huang, L.; Zhu, F.C.; Qu, X.-M.; Sun, S.G. Engineering phase and surface composition of Pt 3 Co nanocatalysts: A strategy for enhancing CO tolerance. *Nano Energy* **2017**, *34*, 224–232. [CrossRef]
58. de la Fuente, J.L.G.; Rojas, S.; Martínez-Huerta, M.V.; Terreros, P.; Peña, M.A.; Fierro, J.L.G. Functionalization of carbon support and its influence on the electrocatalytic behaviour of Pt/C in H2 and CO electrooxidation. *Carbon* **2006**, *44*, 1919–1929. [CrossRef]
59. Urchaga, P.; Baranton, S.; Coutanceau, C.; Jerkiewicz, G. Electro-oxidation of COchem on Pt Nanosurfaces: Solution of the Peak Multiplicity Puzzle. *Langmuir* **2011**, *28*, 3658–3663. [CrossRef]
60. López-Cudero, A.; Cuesta, A.; Gutiérrez, C. Potential dependence of the saturation CO coverage of Pt electrodes: The origin of the pre-peak in CO-stripping voltammograms. Part 1: Pt (111). *J. Electroanal. Chem.* **2005**, *579*, 1–12. [CrossRef]
61. Zamanzad Ghavidel, M.R.; Monteverde Videla, A.H.A.; Specchia, S.; Easton, E.B. The relationship between the structure and ethanol oxidation activity of Pt-Cu/C alloy catalysts. *Electrochim. Acta* **2017**, *230*, 58–72. [CrossRef]
62. Rudi, S.; Cui, C.; Gan, L.; Strasser, P. Comparative Study of the Electrocatalytically Active Surface Areas (ECSAs) of Pt Alloy Nanoparticles Evaluated by Hupd and CO-stripping voltammetry. *Electrocatalysis* **2014**, *5*, 408–418. [CrossRef]
63. Van der Vliet, D.F.; Wang, C.; Li, D.; Paulikas, A.P.; Greeley, J.; Rankin, R.B.; Strmcnik, D.; Tripkovic, D.; Markovic, N.M.; Stamenkovic, V.R. Unique Electrochemical Adsorption Properties of Pt-Skin Surfaces. *Angew. Chem. Int. Ed.* **2012**, *51*, 3139–3142. [CrossRef]
64. Petrii, O.A. The progress in understanding the mechanisms of methanol and formic acid electrooxidation on platinum group metals. *Russ. J. Electrochem.* **2019**, *55*, 3–38. [CrossRef]
65. Zhang, X.; Wang, H.; Key, J.; Linkov, V.; Ji, S.; Wang, X.; Wang, R. Strain Effect of Core-Shell Co@Pt/C Nanoparticle Catalyst with Enhanced Electrocatalytic Activity for Methanol Oxidation. *J. Electrochem. Soc.* **2012**, *159*, B270–B276. [CrossRef]
66. Lin, R.; Cao, C.; Zhao, T.; Huang, Z.; Li, B.; Wieckowski, A.; Ma, J. Synthesis and application of core–shell Co@Pt/C electrocatalysts for proton exchange membrane fuel cells. *J. Power Sources* **2013**, *223*, 190–198. [CrossRef]
67. Jayasayee, K.; Veen, J.A.R.V.; Manivasagam, T.G.; Celebi, S.; Hensen, E.J.M.; de Bruijn, F.A. Oxygen reduction reaction (ORR) activity and durability of carbon supported PtM (Co, Ni, Cu) alloys: Influence of particle size and non-noble metals. *Appl. Catal. B Environ.* **2012**, *111–112*, 515–526. [CrossRef]
68. Jeon, M.K.; Zhang, Y.; McGinn, P.J. A comparative study of PtCo, PtCr, and PtCoCr catalysts for oxygen electro-reduction reaction. *Electrochim. Acta* **2010**, *55*, 5318–5325. [CrossRef]
69. Guterman, V.E.; Belenov, S.V.; Alekseenko, A.A.; Lin, R.; Tabachkova, N.Y.; Safronenko, O.I. Activity and Stability of Pt/C and Pt-Cu/C Electrocatalysts. *Electrocatalysis* **2018**, *9*, 550–562. [CrossRef]
70. Suryanarayana, C.; Norton, M.G. *X-ray Diffraction: A Practical Approach*; Springer: Boston, MA USA, 2013; p. 273. [CrossRef]
71. Gražulis, S.; Daškevič, A.; Merkys, A.; Chateigner, D.; Lutterotti, L.; Quirós, M.; Serebryanaya, N.R.; Moeck, P.; Downs, R.T.; Le Bail, A. Crystallography Open Database (COD): An open-access collection of crystal structures and platform for world-wide collaboration. *Nucleic Acids Res.* **2012**, *40*, D420–D427. [CrossRef]

72. Klug, H.P.; Alexander, L.E. *X-ray Diffraction Procedures from 376 Polycrystalline and Amorphous Materials*; John Wiley: New York, NY, USA, 1974.
73. Shinozaki, K.; Zack, J.W.; Pylypenko, S.; Pivovar, B.S.; Kocha, S.S. Oxygen Reduction Reaction Measurements on Platinum Electrocatalysts Utilizing Rotating Disk Electrode Technique: II. Influence of Ink Formulation, Catalyst Layer Uniformity and Thickness. *J. Electrochem. Soc.* **2015**, *162*, 1144–1158. [CrossRef]